Journal of Sustainable Metallurgy (2023) 9:341–349
https://doi.org/10.1007/s40831-023-00657-6

RESEARCH ARTICLE

Utilization of Vanadium Slag and Iron-Rich Red Mud for the Fabrication of Fe–V Alloy: Mechanism and Performance Analysis

Wei Wang[1,2,3] · **Weibin Wang**[1,2,3] · **Qirui Sun**[1,2,3]

Received: 25 August 2022 / Accepted: 2 February 2023 / Published online: 13 February 2023

Abstract

An innovative technique that provides a new way to use vanadium slag and red mud has been developed. In the proposed method, vanadium slag was used to prepare Fe–V alloys by combining the slag with iron-rich red mud. The effects of the red mud dosage, reduction temperature, and Na_2CO_3 addition on the carbothermal reduction of vanadium slag and iron-rich red mud were investigated. Thermodynamic analysis indicated that optimizing the reduction temperature increased the metal recovery. The roasted samples were tested with X-ray diffraction, scanning electron microscopy, and energy-dispersive X-ray spectroscopy, and the analytical results indicated that a vanadium slag:red mud mass ratio of 40:60 promoted liquid-phase formation and Fe–V alloy grain growth. V and Cr promoted the pearlite transformation and fined the lamellar spacing, imparting higher hardness and improving the electrochemical corrosion resistance of the alloy. Sodium salt addition enhanced the metal recovery by the promoting formation of aluminosilicate slag. This method enables efficient direct reduction of vanadium slag and the production of alloy materials with high added value.

Graphical Abstract

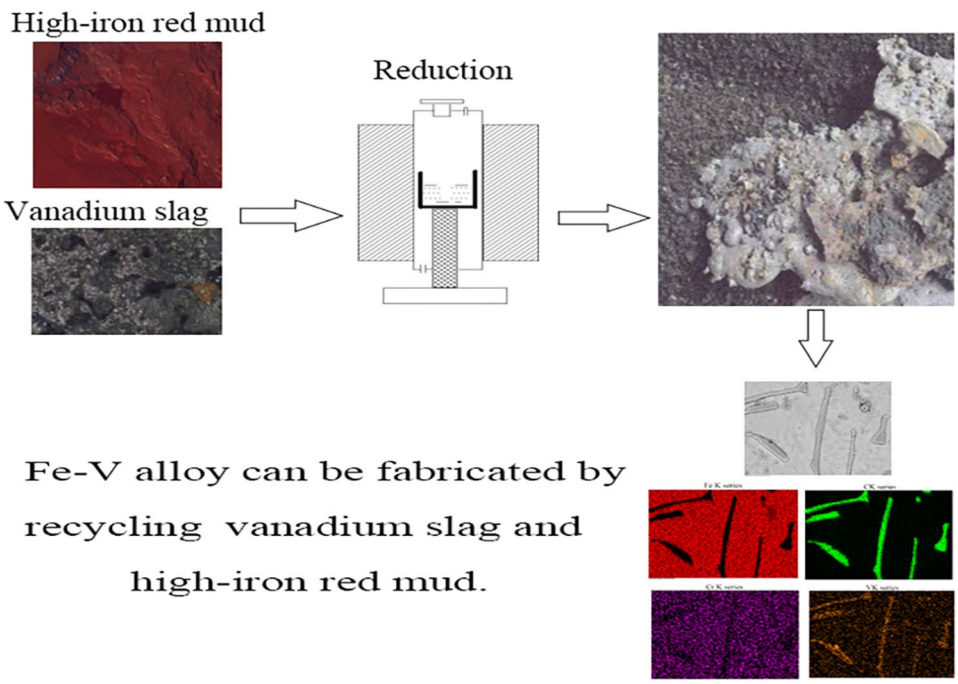

The contributing editor for this article was Adam Clayton Powell.

Extended author information available on the last page of the article

Keywords Fe–V alloy · Corrosion resistance · Vanadium slag · Carbothermal reduction · Iron-rich red mud

Introduction

Vanadium is an important steel additive and is generally used to improve the strength and weight relationships of qualified steels. Vanadium-alloyed ferrite–pearlite steels are widely used in buildings, bridges, pipelines, and ships [1, 2]. The average vanadium content of the Earth's crust is approximately 0.0015%; therefore, most vanadium is extracted from vanadium slag. In this process, an additive such as NaCl or CaO is blended with the vanadium slag. The blend is converted to water-soluble sodium vanadates by calcination and then leached with an aqueous acid solution. Vanadium oxides are obtained by purifying the vanadium deposits, roasting, and reduction [3, 4]. Waste gases such as SO_2, SO_3, Cl_2, and HCl are discharged during the reduction process, and this causes serious environment pollution. The process also consumes substantial amounts of additives. The development of a simple and environmentally friendly method for recycling vanadium from vanadium slag is therefore needed to overcome these problems.

Recently, a technique for preparing ferroalloys by high-temperature carbothermal reduction smelting has received much attention because of its high reduction degree and strong raw material adaptability. He and Zeng successfully prepared low Ni–Cr alloy cast iron by high-temperature carbothermal reduction of a laterite ore and red mud (RM) [5]. The alkali-metal oxides in RM promote crystal particle growth and metal recovery. Some studies have investigated the use of sodium carbonate to enhance metal recovery during iron-rich RM reduction roasting [6, 7]. Using a combination of vanadium slag and iron-rich RM to prepare alloys by high-temperature carbothermal reduction is feasible and economical. Bauxite residue is sometimes referred to as 'red mud' and is used in several publications. During alumina production by the Bayer process, a large quantity of RM, which contains large amounts of Al_2O_3, SiO_2, and alkali-metal oxides, is generated [8, 9]. Recovering valuable metals from RM has become a hot topic in terms of decreasing the environmental pollution. The production of ferrovanadium alloys by recycling a mixture of vanadium slag and iron-rich RM has rarely been reported.

In this study, a blend of RM and vanadium slag was used to synthesize high-strength Fe–V alloys via high-temperature carbothermal reduction smelting. The alloys obtained via this process contain about 8% V and 81% Fe. The relationship between the corrosion behavior of the alloy and its microstructure, and the effects of sodium carbonate addition on metal recovery and the mechanical properties of the alloy were investigated. The thermodynamic analysis results and the mechanical properties of the obtained Fe–V alloys will be useful in developing further methods for recycling vanadium slag and iron-rich RM by carbothermal reduction smelting.

Materials and Methods

Materials

The vanadium slag and iron-rich RM used in this work were obtained from the Kunming Iron & Steel Co., Ltd. (Kunming City, Yunnan province, P. R. China) and the Henan Aluminum Co., Ltd. (Zhengzhou, P. R. China), respectively. Table 1 shows the main components of the vanadium slag and iron-rich RM. Coke powder was used as a reductant in the carbothermal reduction of vanadium slag and RM. Table 2 shows details of the coke composition. Sodium carbonate (Na_2CO_3) with the particle size of 50–74 μm was of analytical grade (Sinopharm, China).

Experimental Methods

The vanadium slag, coke powder and iron-rich RM were ground to particles of size less than 150 μm and then wet mixed with 0.5% of bentonite as the binder and right amount of water in a disk pelletizer with diameter of 1 m and thickness of 0.15 m at a speed of 40 rpm and an angle of 47° to the surface. The addition of coke powder was 40 wt% of the vanadium slag. The iron-rich RM additions varied from 40 to 150 wt% of the vanadium slag. Each pellet had a mass of about 400 g. All the samples are denoted by V_xR_y, where V

Table 2 Chemical compositions analysis of the coke (wt%)

Fixed carbon	Volatiles matter	Ash	Moisture	S	P
83.18	3.57	9.86	2.11	0.49	0.51

Table 1 Chemical compositions analysis of vanadium slag and iron-rich RM (wt%)

Materials	Fe_2O_3	V_2O_5	Cr_2O_3	SiO_2	Al_2O_3	CaO	TiO_2	MgO	Na_2O	LOI
Iron-rich RM	39.62	–	–	16.48	15.63	13.32	3.28	2.37	3.76	5.54
Vanadium slag	35.63	16.48	9.38	14.32	4.35	3.06	11.46	3.66		1.66

Table 3 Chemical compositions of the pellets studied (wt%)

Number	Vanadium slag	RM	Coke	Na_2CO_3
$V_{40}R_{60}$	31.38	47.07	12.55	9
$V_{50}R_{50}$	37.92	37.92	15.16	9
$V_{60}R_{40}$	44.03	29.35	17.62	9
$V_{70}R_{30}$	49.77	21.33	19.9	9

stands for vanadium slag, R stands for RM, and *x*:*y* is their mass ratio in the samples (Table 3). Direct reduction of the pellets was performed in a high-temperature muffle furnace with a $MoSi_2$ heating element in air atmosphere. The reduction temperature was varied in the range of 1500–1600 °C for a period of 100 min. After reduction, the sample was cooled to ambient temperature and removed from the furnace. Then, the reduced pellets were crushed and ground to below 45 μm size in the grinding mill. To obtain the products, magnetic separation tests were carried out in an XCGS-73 Davis Magnetic Tube using a magnetic field intensity of 0.1 Tesla. The amount of metal obtained from the vanadium slag and iron-rich RM is

$$\eta = \frac{m_F \omega_F}{m_V \alpha_V + m_R \alpha_R}, \quad (1)$$

where η is the metal recovery efficiency, m_F is the mass of the alloy products, ω_F is the amount of metal in the alloy products, α_V and α_R are the contents of vanadium or iron in the vanadium slag and iron-rich RM, respectively, and m_V and m_R are the masses of vanadium slag and iron-rich RM, respectively.

Microstructural Characterization

The phases in the reduced slag were determined by an X-ray diffractometer (XRD, Bruker D8) using Cu Kα radiation. The surface morphologies and element distributions in the alloy samples were investigated by scanning electron microscopy (SEM, Japan, JSM-5610LV) combined with energy-dispersive X-ray spectroscopy (EDS, INCA Energy 350). The cross-sectional microhardness was measured at six points on the specimen with a Vickers hardness tester under an applied load of 100 g (HV0.1) for 15 s each.

The corrosion behaviors of the alloys were evaluated by potentiodynamic polarization. The polarization curves for each specimen were recorded in 0.1 M NaCl solution by using an Autolab PGSTAT128N electrochemical testing system. The tests were performed with a three-electrode cell with a platinum counter electrode, a saturated calomel reference electrode, and the specimen sealed in epoxy resin, with an exposed testing area of 1 cm^2, as the working electrode. The polarization curves were recorded after a steady-state potential had been achieved; the scanning rate was 20 mV/min and the scanning range was from − 1.4 to 0.2 V.

Results and Discussion

Effect of Reduction Behavior of Raw Material

Thermodynamic analysis was used to investigate the reduction behaviors of the vanadium slag and RM during carbothermal reduction. The reduction reactions that are probably involved in this system are as follows [10].

$$V_2O_{3(S)} + 3C = 2[V] + 3CO_{(g)} \quad (2)$$

$$VO_{(S)} + C = [V] + CO_{(g)} \quad (3)$$

$$Fe_2O_{3(S)} + 3C = 2[Fe] + 3CO_{(g)} \quad (4)$$

$$Cr_2O_{3(S)} + 3C = 2[Cr] + 3CO_{(g)} \quad (5)$$

FactSage thermodynamic software was used to perform thermodynamic calculations on the above reactions. The temperature dependences of the Gibbs free energies (ΔG^{θ}) for reactions (2)–(5) over various temperature ranges were plotted (Fig. 1). The Gibbs free energies for the reduction reactions of the metal oxides in RM and the vanadium slag all decreased with increasing temperature. This indicates that increasing the reduction temperature can promote these reduction reactions. Cost is an important factor in industrial processes; therefore, the optimum temperature range for the reduction reactions is 1500–1550 °C. As shown in the Fe–V binary phase diagram (Fig. 2), an alloy undergoes the phase transformation from the high-temperature L phase to the low-temperature α phase. The presence of a Fe-rich phase in the Fe–V alloy system indicates that a Fe–V alloy can be

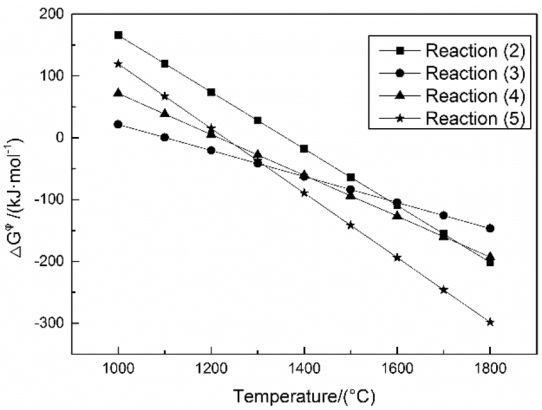

Fig. 1 ΔG^{θ} for reduction reactions on temperature

obtained via an isomorphous transformation in this temperature range [11, 12].

Figure 3 shows SEM image with the elemental distributions in the alloys obtained from a vanadium slag:RM mass ratio of 60:40, with the addition of 9% Na_2CO_3, after reduction at 1550 °C for 100 min. Notably, the reduction products from the mixture contain Fe and C, along with V and Cr, and the precipitate phase has the highest carbon enrichment. Each product is about 95 g, accounting for just under a quarter of the mass in the mixture. Generally, the Fe content is the highest, and the amounts of V and Cr are relatively low. Because of the even distribution of alloy elements in the matrix, it has a uniform and integrated structure, which contributes to improvements in the hardness and mechanical performance of the Fe–V alloy [13].

Influence of Reduction Temperature

The effects of the reduction temperature on vanadium and iron mineral reduction were investigated at a vanadium slag:RM mass ratio of 60:40, with the addition of 9% Na_2CO_3. The results are shown in Fig. 4.

Figure 4 shows that the recovery of vanadium and iron increased with increasing temperature, suggesting that a high temperature effectively promoted reduction reactions [14]. As Cr_2O_3 was deoxidized easily, the change of chromium recovery was same as that of iron. However, the recovery of vanadium and iron increased only slightly between 1550 and 1600 °C. This is because at temperatures greater than 1550 °C, fayalite or hercynite was generated from FeO, SiO_2, and Al_2O_3, and inhibited reduction of the mixture [6]. However, Na_2O can react with SiO_2 prior to FeO, improving the reduction of iron minerals. Therefore, the pellets with high basicity benefit the reduction of vanadium and iron ores in RM and vanadium slag. In industrial practice, the higher was the reduction temperature, the higher were the production costs. The optimum temperature was therefore 1550 °C.

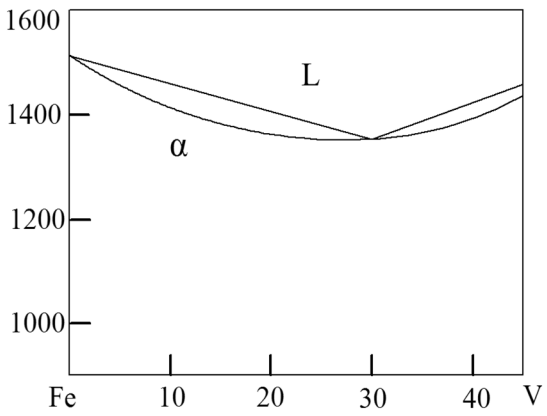

Fig. 2 A Fe-rich portion of the Fe–V alloy system

Effect of Sodium Carbonate Dosage

The mechanism of direct reduction with sodium carbonate as an additive was clarified by investigating the phase transformations of mixtures with various sodium carbonate dosages. Figure 5 shows the XRD patterns of slags that were reduced with various sodium carbonate dosages. The vanadium slag contains ferric oxide and chromic oxide. The mineral phases present in the four reduced samples clearly differ. The diffraction peaks corresponding to hematite and quartz gradually weakened, and those corresponding to sodium aluminosilicate ($NaAlSiO_4$) strengthened, with increasing sodium carbonate dosage. The obvious shift of the ferric oxide and chromic oxide indicates a significant change of their composition, suggesting the formation of a ferroalloy. However, the peak intensities of titanium dioxide remain relatively constant. In addition, the diffraction peaks of hercynite phase appear in slags without sodium carbonate, which is produced by the reaction between ferric oxide and aluminum oxide. There are two reasons for this. First, according to Eqs. (6)–(8), hematite and quartz were transformed into metallic iron and sodium aluminosilicate, respectively, by sodium carbonate addition [15, 16]. Meanwhile, iron within the hercynite was also reduced into metallic iron. Second, Na_2CO_3 addition can generate a liquid phase and facilitate the growth of metallic iron particles during gas-based direction reduction [17, 18]; this is conducive to ferrovanadium particle aggregation. The amounts of sodium aluminosilicate and quartz in the slag increased, which promoted the recovery of iron and vanadium. Subsequently, we used specimens sintered with 9% Na_2CO_3 at 1550 °C to investigate the alloy formation process.

The reduced slag contained a large amount of aluminosilicate, and therefore, ceramic materials with excellent properties were synthesized by high-temperature sintering of the residues. The method developed in this study enables comprehensive use of vanadium slag and RM and therefore provides a long-term effective solution for recycling two industrial wastes.

$$Fe_2O_3 + CO \rightarrow 2FeO + CO_2 \quad (6)$$

$$FeO + Al_2O_3 \rightarrow FeO \cdot Al_2O_3 \quad (7)$$

$$FeO \cdot Al_2O_3 + Na_2O + SiO_2 + CO \rightarrow Fe + NaAlSiO_4 + CO_2 \quad (8)$$

Characterization of Alloy Samples with Different Vanadium Slag: Red Mud Mass Ratios

Figure 6 shows the microstructures of samples with different vanadium slag:RM mass ratios after carbothermal

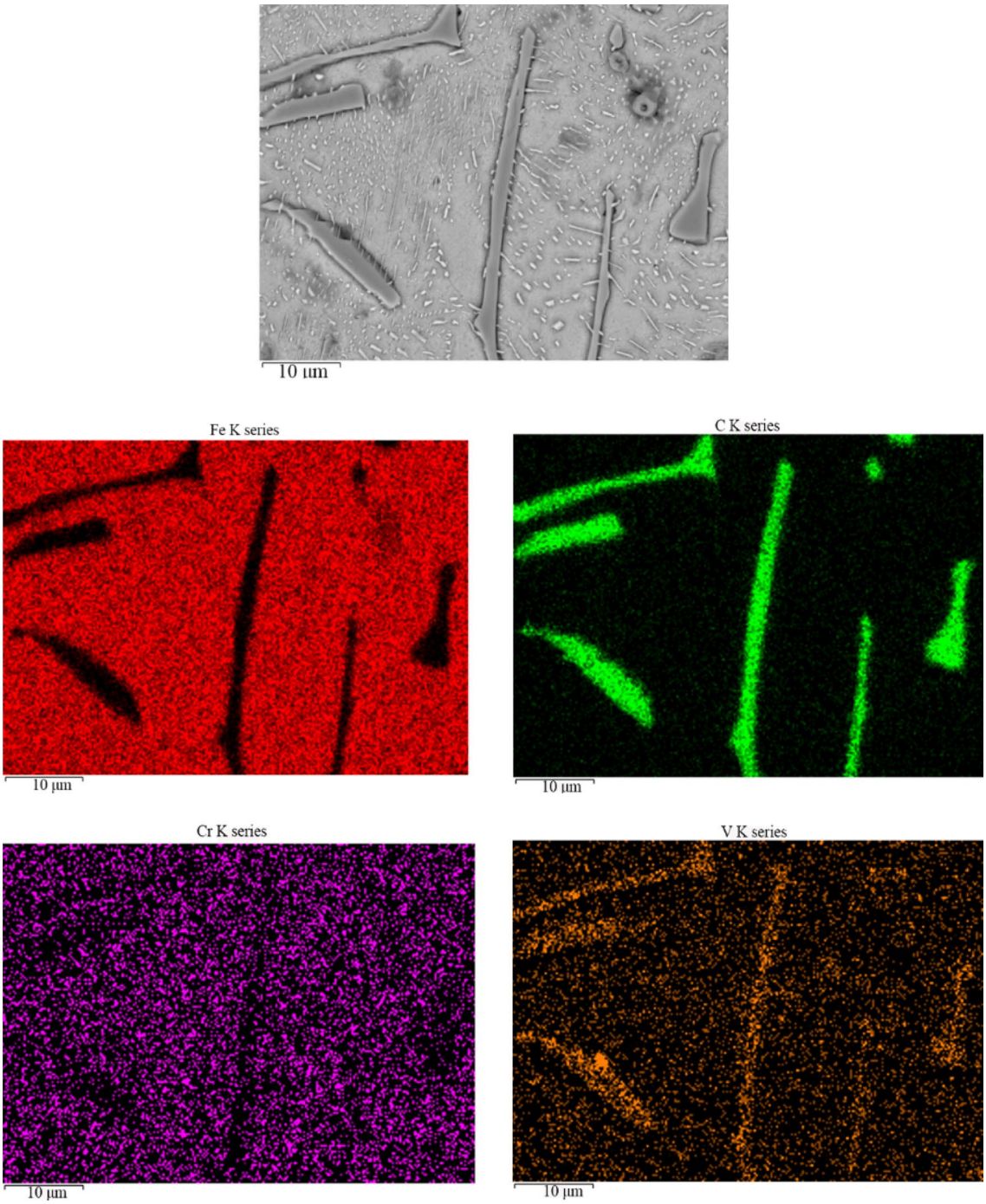

Fig. 3 SEM image and corresponding Fe, C, Cr, and V elemental distribution of Fe–V alloy

reduction at 1550 °C for 100 min. The microstructures of the four specimens consisted of a ferrite matrix, with lamellar pearlite and dispersed carbides, which were distributed mainly as a grid with boundaries of metallic particles. However, because the alloy contents differed, there are clear differences among the quantities and distributions of the microstructures. Lamellar pearlite formation increased with increasing vanadium slag:RM mass ratio from 40:60 to 60:40. There are two reasons for this. First, the amounts of V and Cr in the alloy increase markedly with increasing amount of vanadium slag in the mixture. Second, with perfect separation of Fe, Cr, and V elements and the slag phases, Fe–V alloy is easily formed during the reduction process. The vanadium slag is adequately incorporated into the RM with high contents of CaO and Na_2O, which is conducive to recovery of the alloy elements. In addition, the

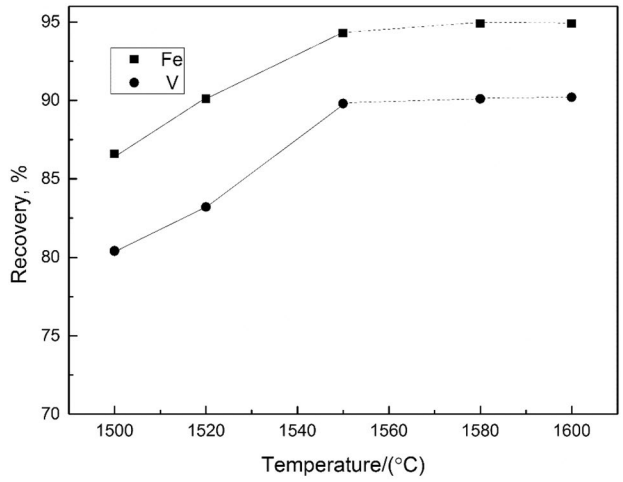

Fig. 4 The metal recovery of ferrovanadium products at different temperatures

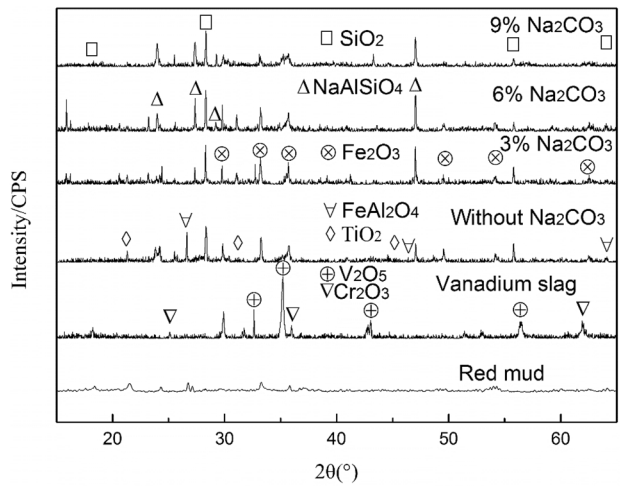

Fig. 5 XRD patterns of mixtures reduced with various sodium carbonate dosages

low-temperature flux (i.e., K_2O and Na_2O) from the RM contributes to liquid-phase formation, which can promote gas-particle flow and improve the reaction conditions. The increased amounts of V and Cr in the alloy generated large quantities of increasingly fine pearlite via an austenite transformation [19, 20]. This is because Cr and V can enlarge the pearlite transformation field and decrease the velocity of pearlite nodule development, respectively. V can refine the entire transformed microstructure and also reduce the lamellar spacing of pearlite. However, with further increases in the vanadium slag:RM mass ratio, more hard carbides appeared in the alloy. This could adversely affect the mechanical performance of the alloy [21, 22]. A certain amount of metal carbides is generally formed along the crystal particles during solidification. Use of an appropriate amount of RM is therefore important for achieving complete carbothermal reduction. Tables 4 and 5 show the chemical composition of the reduced slag and Fe–V alloy for these samples, respectively. Obviously, the contents of V_2O_5, Cr_2O_3, and Fe_2O_3 in the reduced slag are all significantly increased, which changes with the increasing of vanadium slag, and have the same variation tendency with the metal recovery.

Mechanical Performance of Fe–V Alloys

Figure 7 shows the Fe–V alloy hardness values. The error bar shows the standard deviation across five independent samples. The alloy hardness clearly increased with increasing pearlite content. This is closely related to the amount of vanadium in the alloy. As the vanadium content increased, the particle sizes of ferrite and pearlite in the alloys decreased, increasing the alloy hardness [23]. In addition, these alloy elements can promote the transformation of austenite near small carbide particles into lamellar pearlite. This suggests that vanadium decreases the remaining amount of austenite and therefore increases the hardenability of the alloy. However, when the vanadium content is greater than 4%, it easily forms chemical compounds, such as Cr, V carbides, and $(Cr, Fe)_{23}C_6$ carbides, along the austenite grains during natural cooling [24, 25], which decreases the alloy hardness.

Polarization of Fe–V Alloys

Figure 8 shows the potentiodynamic polarization curves for Fe–V alloys in 0.1 M NaCl solution at 25 °C. The electrochemical parameters listed in Table 6 were determined by the Tafel extrapolation method. The lowest corrosion current density and the highest corrosion potential clearly show that $V_{60}R_{40}$ gives the highest resistance to electrochemical corrosion. In contrast, $V_{70}R_{30}$ is easily corroded, showing that the alloy microstructure plays an important role in the corrosion behavior. The Cr and V from vanadium slag help to improve the corrosion resistance of the alloy. A previous study showed that a primary battery develops easily at a ferrite–graphite interface. The addition of excess reductant caused the formation of graphite and hard carbides in $V_{70}R_{30}$ [5]; it is therefore susceptible to corrosion.

Conclusion

A novel environmentally friendly process, which is based on high-temperature carbothermal reduction smelting, for producing Fe–V alloys from vanadium slag and iron-rich RM was developed. The optimum conditions for alloy preparation were a vanadium slag:RM mass ratio of 60:40 and 9% Na_2CO_3 addition. The obtained Fe–V alloy gave an excellent

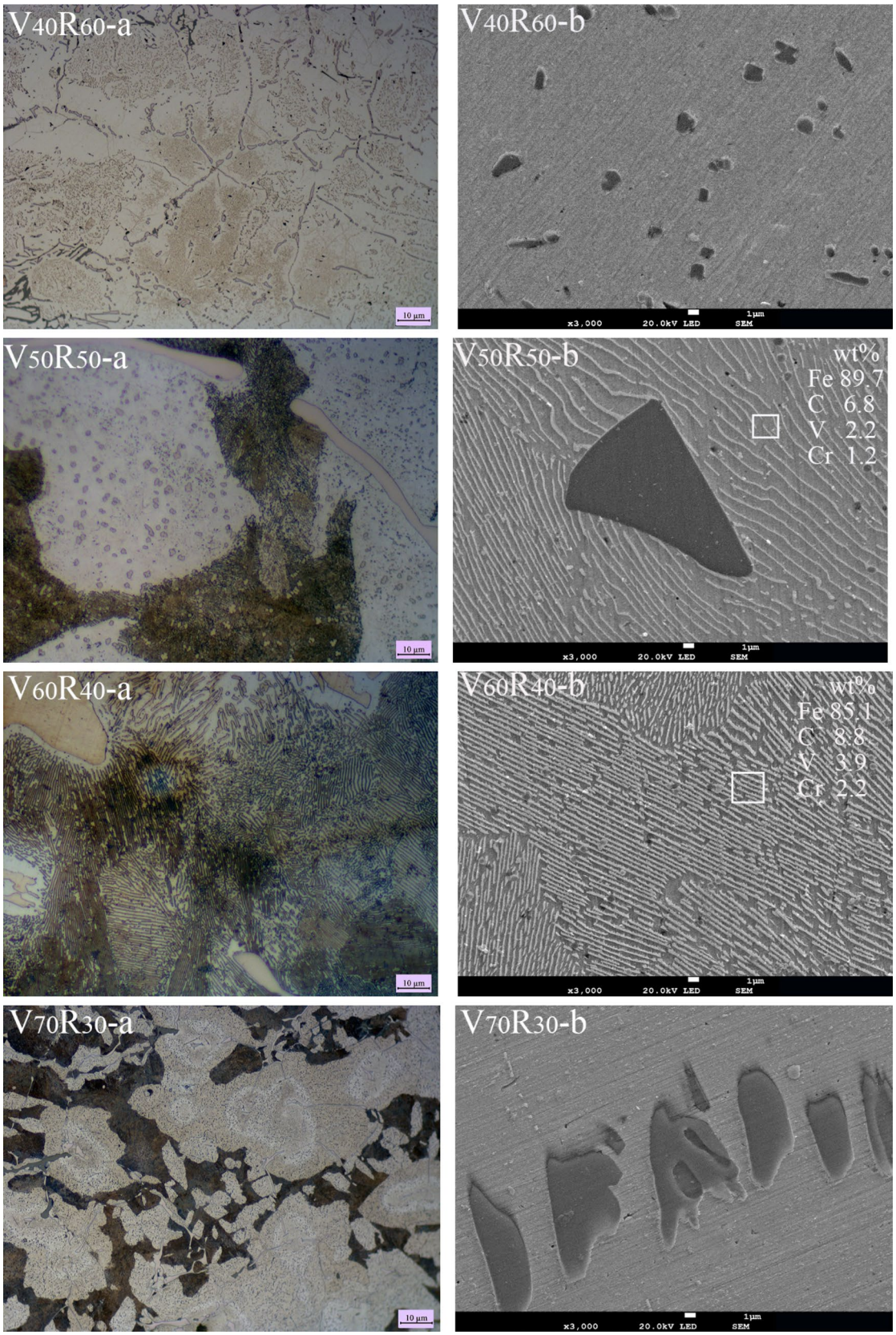

Fig. 6 Microstructures and EDS results of samples with various RM dosage

Table 4 Chemical analysis of the reduced slag (wt%)

Samples	Na_2O	Al_2O_3	SiO_2	FeO	V_2O_5	Cr_2O_3	CaO	TiO_2	MgO
$V_{40}R_{60}$	14.32	25.64	19.6	5.01	2.06	1.02	18.52	10.77	3.06
$V_{50}R_{50}$	14.16	25.25	19.5	5.12	2.13	1.16	17.36	11.23	4.09
$V_{60}R_{40}$	13.88	24.62	19.8	5.23	2.32	1.42	17.22	11.48	4.03
$V_{70}R_{30}$	13.38	24.11	19.3	5.28	2.58	1.72	16.86	11.86	4.91

Table 5 Chemical analysis of the Fe–V alloy (wt%)

Samples	C	V	Cr	Si	S	P	Fe
$V_{40}R_{60}$	4.56	7.82	3.06	0.25	0.043	0.042	84.22
$V_{50}R_{50}$	4.42	8.44	4.89	0.27	0.036	0.038	81.91
$V_{60}R_{40}$	4.09	11.28	5.12	0.28	0.041	0.042	79.15
$V_{70}R_{30}$	3.31	12.82	5.18	0.32	0.034	0.044	78.28

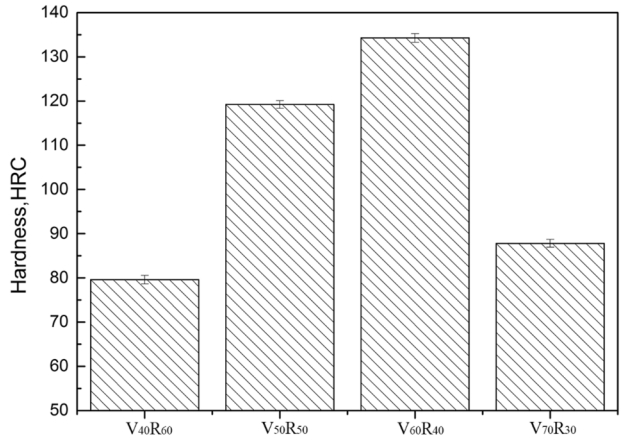

Fig. 7 Vickers hardness of samples with various vanadium slag:RM mass ratios

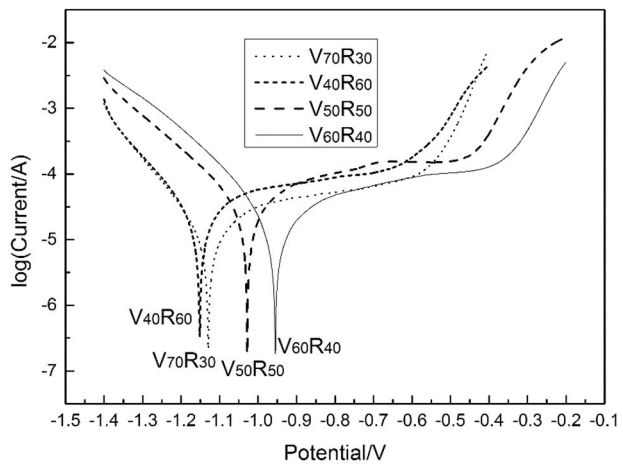

Fig. 8 Potentiodynamic polarization diagram for the Fe–V alloys

Table 6 Electrochemical parameters of the Fe–V alloys

	$V_{40}R_{60}$	$V_{50}R_{50}$	$V_{60}R_{40}$	$V_{70}R_{30}$
I_{corr}/μA/cm^2	31.17	14.21	12.33	23.41
E_{corr}/mV	− 1164	− 1022	− 941	− 1142

overall performance, with high hardness and good corrosion resistance. This method solves the problem of vanadium slag and RM disposal and enables sustainable production to be achieved.

High temperatures promoted the reactions of iron oxides and vanadium oxides and increased the recovery of iron and vanadium in the alloy during reduction. For industrial applications, the optimum temperature for carbothermal reduction is 1550 °C. Because of the low price of the main materials, which are industrial wastes, the alloy can potentially be used as a supplementary material in engineering industries.

An appropriate amount of sodium carbonate enhanced the reduction of iron oxides and vanadium oxides and facilitated alloy grain growth.

The microstructures of the Fe–V alloys obtained from vanadium slag and iron-rich RM, especially primary cementite and pearlite, are significantly affected by V. An appropriate distribution of hard carbides can endow the Fe–V alloy with good mechanical properties. Such alloys could be widely used in high-temperature materials without creating new residues.

Acknowledgements This work was financially supported by Natural Science Foundation of Henan province [Grant Number 222300420437].

Declarations

Conflict of interest The authors declare that they have no conflict of interest.

References

1. Diao J, Liu L, Lei J, Tan WF, Li HY, Xie B (2021) Oxidation mechanism of vanadium slag with high MgO content at high temperature. Metall Mater Trans B 52:494–501
2. Fang HX, Li HY, Zhang T, Liu BS, Xie B (2015) Influence of CaO on existence form of vanadium-containing phase in vanadium slag. ISIJ Int 55:200–206
3. Semykina A, Dzhebian I, Shatokha V (2012) On the formation of vanadium ferrites in $CaO–SiO_2–FeO–V_2O_5$ slags. Steel Res Int 83:1129–1134
4. Li KQ, Jiang Q, Gao L, Chen J, Peng JH, Koppala S, Omran M (2020) Investigations on the microwave absorption properties and thermal behavior of vanadium slag: improvement in microwave oxidation roasting for recycling vanadium and chromium. J Hazard Mater 395:122698
5. He A, Zeng J (2017) Direct preparation of low Ni–Cr alloy cast iron from red mud and laterite nickel ore. Mater Des 115:433–440
6. Zhu DQ, Chun TJ, Pan J, He Z (2012) Recovery of iron from high-iron red mud by reduction roasting with adding sodium salt. J Iron Steel Res Int 19:1–5
7. Guo YH, Gao JJ, Xu HJ, Zhao K, Shi XF (2013) Nuggets production by direct reduction of high iron red mud. J Iron Steel Res Int 20:24–27
8. Alam S, Das SK, Rao BH (2019) Strength and durability characteristic of alkali activated GGBS stabilized red mud as geomaterial. Constr Build Mater 211:932–942
9. Chowdhury AR, Jaksik J, Hussain I, Longoria R, Faruque O, Cesano F, Scarano D, Parsons J, Uddin MJ (2019) Multicomponent nanostructured materials and interfaces for efficient piezoelectricity. Nano-Struct Nano-Objects 17:148–184
10. Wang S, Guo YF, Zheng FQ, Chen F, Yang LZ, Jiang T, Qiu GZ (2020) Behavior of vanadium during reduction and smelting of vanadium titanomagnetite metallized pellets. Trans Nonferrous Met Soc China 30:1687–1696
11. Ustinovshikov Y, Pushkarev B, Sapegina I (2005) Phase transformations in alloys of the Fe–V system. J Alloy Compd 398:133–138
12. Park J, Shim JH, Lee YK (2016) Room-temperature solid solution softening in Fe–V binary system. Met Mater Int 22:1–7
13. Wang ZH, Hui WJ, Chen Z, Zhang YJ, Zhao XL (2020) Effect of vanadium on microstructure and mechanical properties of bainitic forging steel. Mater Sci Eng A 771:138653
14. Liu W, Yang J, Xiao B (2009) Application of Bayer red mud for iron recovery and building material production from alumosilicate residues. J Hazard Mater 161:474–478
15. Li XB, Xiao W, Liu W, Liu GH, Peng ZH, Zhou QS, Qi TG (2009) Recovery of alumina and ferric oxide from Bayer red mud rich in iron by reduction sintering. Trans Nonferrous Met Soc China 19:1342–1347
16. Li ZF, Zhang J, Li SC, Lin CJ, Gao YF, Liu C (2020) Feasibility of preparing red mud-based cementitious materials: synergistic utilization of industrial solid waste, waste heat, and tail gas. J Clean Prod 285:124896
17. Wang XP, Sun TC, Kou J, Li ZC, Tian Y (2018) Feasibility of co-reduction roasting of a saprolitic laterite ore and waste red mud. Int J Miner Metall Mater 25:591–597
18. Li GH, Jun L, Peng ZW, Zhang YB, Rao MJ, Jiang T (2015) Effect of quaternary basicity on melting behavior and ferronickel particles growth of saprolitic laterite ores in Krupp-Renn process. ISIJ Int 55:1828–1833
19. Cao HT, Dong XP, Chen SQ, Dutka M, Pei YT (2017) Microstructure evolutions of graded high-vanadium tool steel composite coating in-situ fabricated via atmospheric plasma beam alloying. J Alloys Compd 720:169–181
20. Grudinsky P, Zinoveev D, Yurtaeva A, Kondratiev A, Dyubanov V, Petelin A (2021) Iron recovery from red mud using carbothermic roasting with addition of alkaline salts. J Sustain Metall 7:858–873
21. Li Y (2010) The effects of V on phase transformation of high carbon steel during continuous cooling. Acta Metall Sin 46:1501–1510
22. Niu G, Chen YL, Wu HB, Wang X, Zuo MF, Xu ZJ (2016) Effects of chromium, vanadium and austenite deformation on transformation behaviors of high-strength spring steels. J Iron Steel Res Int 23:1323–1332
23. Sourmail T, Garcia-Mateo C, Caballero FG, Cazottes S, Epicier T, Danoix F, Milbourn D (2017) The influence of vanadium on ferrite and bainite formation in a medium carbon steel. Mater Sci Eng A 48:3985–3996
24. Todić A, Čikara D, Pejović B, Todić T, Čamagić I, Mićić V, Yusup S (2017) The influence of the vanadium content on the toughness and hardness of wear resistant high-alloyed Cr–Mo steel. FME Trans 45:130–134
25. Li YJ, Dong SY, Yan SX, Liu XT, He P, Xu BS (2018) Microstructure evolution during laser cladding Fe–Cr alloy coatings on ductile cast iron. Opt Laser Technol 108:255–264

Authors and Affiliations

Wei Wang[1,2,3] · Weibin Wang[1,2,3] · Qirui Sun[1,2,3]

✉ Wei Wang
wwlyzwkj@126.com

[1] College of Materials Science and Engineering, Henan University of Science and Technology, Luoyang 471023, Henan, People's Republic of China

[2] Collaborative Innovation Center of Nonferrous Metals Henan Province, Luoyang 471023, Henan, People's Republic of China

[3] Henan Key Laboratory of Non-ferrous Materials Science & Processing Technology, Luoyang 471023, Henan, People's Republic of China